Ultrafast carrier dynamics near the Si(100)2×1 surface

Seongtae Jeong
Center for X-Ray Optics, Lawrence Berkeley National Laboratory, 1 Cyclotron Road, Berkeley, California 94720

Jeffrey Bokor
Department of Electrical Engineering and Computer Science, University of California, Berkeley, California 94720
(Received 8 September 1998)

We present a time-resolved photoemission study of carrier dynamics near the Si(100)2×1 surface. It is found that the dominant contribution to the photoemission process originates from defect states on the Si(100)2×1 surface. Enhanced optical absorption is observed for these defect states and carrier exchange between these states and the bulk is observed. The electron density near the surface and the shape of the electron energy distribution are found to change on a very fast time scale. A simple theoretical model is established to extract transport parameters from the observed electron energy distribution.
[S0163-1829(99)07107-6]

I. INTRODUCTION

The study of the transport properties of semiconductor materials is a very active research area not only due to numerous scientific and practical applications for various electronic and optical devices but also due to novel physical phenomena found in their heterostructures and nanostructures. Especially, the study of the transport properties of silicon has been very actively pursued because it has been the material of choice for modern integrated circuit technology. The theoretical description of carrier transport inside a silicon electronic device has been largely based on simple sets of linear differential equations referred to as ''drift-diffusion equations'' in which the energy distribution of carriers is assumed to be thermal. However, as modern electronic devices are scaled down to an ever-smaller dimension and their operating speeds become faster, the carriers are subject to a strong spatiotemporal gradient of electric field, rendering the validity of the drift-diffusion equations approach and the assumption of equilibriated carrier distribution questionable. In fact, a number of new phenomena have been attributed to the presence of a nonthermal or hot-electron distribution of carriers and a detailed microscopic understanding of the carrier dynamics in this hot-electron regime is needed for proper modeling of these hot-electron phenomena.[1]

To study carrier transport occurring on a very short time scale in the direct time domain, a very powerful approach employing state-of-the-art short pulse laser technology has been used. Because the time scale accessible with ultrafast laser spectroscopic techniques approaches or even exceeds that of the fundamental scatterings in semiconductors, they have provided valuable insights into the carrier dynamics before carriers reach an equilibrium state.[2] However, this technique was mainly applied to direct band-gap materials such as GaAs. The difficulty of applying ultrafast laser spectroscopic techniques to indirect band-gap materials such as silicon is simply that the momentum-conserving phonon involved in the fundamental optical transition makes it hard to relate observed experimental changes in optical properties to changes in the carrier distribution.

As one of the ultrafast spectroscopic techniques, time-resolved multiphoton photoemission spectroscopy has a potential to become a particularly effective tool in overcoming this. Photoemission spectroscopy can directly probe the electron energy distribution inside the solid. Furthermore, the angle-resolved detection capability of photoemission spectroscopy can be used to probe different parts of the Brillouin zone.[3] The surface sensitivity of photoemission spectroscopy[4] can be a valuable tool for studying physics or carrier dynamics near the surface where the presence of the band-gap states plays an important role.[5] There are quite a few studies of ultrafast carrier dynamics in silicon using multiphoton photoemission spectroscopy with various pulsed laser systems.[6–9]

After a preliminary result of ultrafast carrier dynamics near the Si(100)2×1 surface was reported in Ref. 6, we have performed a more detailed and quantitative study on the nature of the states involved in the photoemission, the origin of fast decay observed in states near the conduction-band minimum (CBM), the temporal evolution of the electron temperature and its pump beam fluence dependence. In Sec. II of this paper, a description of the experimental setup is given. In Sec. III, the time-resolved spectra are presented and the nature of the states observed in the experiments is discussed using the symmetry property of the observed states and the substrate temperature dependence of the photoemission yield. In Sec. IV, various processes involving linear optical absorption, nonlinear optical absorption, surface recombination and the diffusion of carriers from the surface state into the bulk states are shown to coexist on an ultrafast time scale. It is shown how the carrier distribution evolves from the initial nonthermal distribution to a thermal one, and the fluence dependence of the electron energy distribution is discussed. An effective electron temperature at each stage of electron energy distribution evolution is extracted by fitting the experimental data to a Maxwell-Boltzmann distribution. A simple theoretical model is presented to extract useful dynamical parameters such as the electron energy relaxation time.

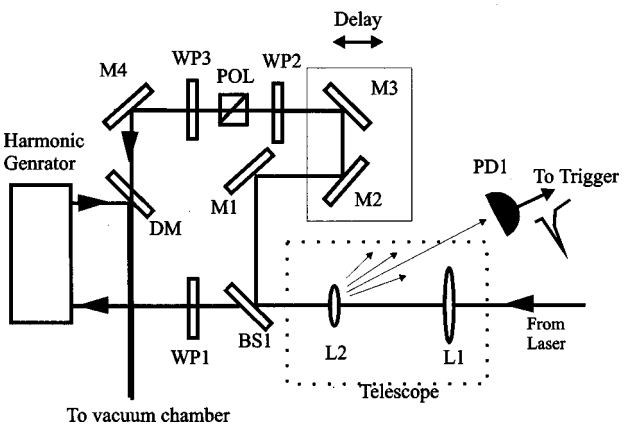

FIG. 1. Optics layout before the vacuum chamber. (L1, L2: telescope lens; PD1: photodiode; BS1: beam splitter; M1, M2, M3, M4: mirror; WP1, WP2, WP3: wave plate; POL: polarizer; DM: dichroic mirror.)

II. EXPERIMENTAL SETUP

The experimental setup is similar to the one described in previous publications.[6,10] The laser system is a Ti:sapphire regenerative amplifier system delivering 150 fsec pulses of energy greater than 0.5 mJ per pulse at 1 kHz. The laser beam is transported to the vacuum chamber using various optical components. The schematic of the optics layout is presented in Fig. 1. A 50/50 beam splitter (BS1) splits the optical pulse into two pulses of equal energy. One pulse referred to as ''pump beam'' travels through the optical delay line and eventually it is delivered to the sample inside a vacuum chamber. The polarization of the pump beam can be varied by rotating the half wave plate (WP3) and its intensity can be varied by using a half wave plate (WP2) and a thin-film polarizer (POL) combination. The second pulse is used to generate the third-harmonic pulse (266 mm) through the harmonic generator. The 266-nm pulse is referred to as a ''probe beam.'' The probe pulse (266 nm) and pump pulse (800 nm) are aligned to travel collinearly toward the sample inside the vacuum chamber using a dichroic mirror (DM).

The vacuum chamber is equipped with low-energy electron diffraction (LEED) and an electron spectrometer. The pressure inside the chamber is kept below 5×10^{-11} Torr. The energy of the photoemitted electrons is measured using the time-of-flight technique.

For the experiments described in this paper, three different Si(100) samples are used to satisfy certain experimental requirements. Table I shows the doping density, resistivity, and miscut with respect to the Si(100) face. From the resistivity of each sample provided by the manufacturer, the doping density is calculated by using mobility values given in the literature.[11]

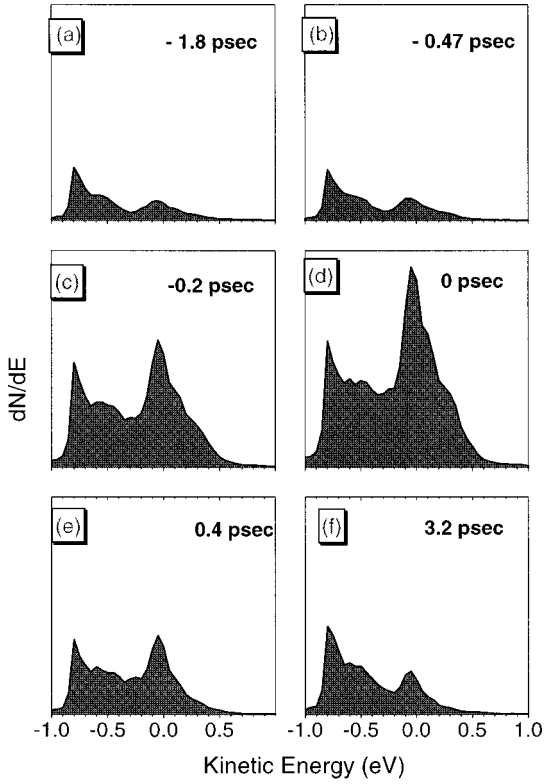

FIG. 2. Time-resolved spectra for different time delays are shown. The pump probe time delay is specified for each plot.

Before introduction into the chamber, the samples are solvent rinsed and then the native oxide on the surface is removed by dipping into a buffered HF solution. After an HF dip, the surface of the sample is terminated with hydrogen, which is evidenced by the dewetting of the surface. The sample is mounted on the *XYZ* sample manipulator immediately after HF cleaning and deionized water rinsing. Once the pressure of the vacuum chamber reaches 5×10^{-11} Torr after bakeout, the sample is cleaned by heating to 1300 K for two minutes using the electron-beam heater. After slowly cooling the sample to room temperature at a rate of 20 K per minute, a very sharp 2×1 LEED pattern is observed. The LEED pattern survives a few weeks but the sharpness of the pattern degrades with time. The LEED pattern becomes sharp again after annealing the sample at 1000 K. The LEED pattern is monitored after each run of the experiment.

III. NATURE OF INITIAL STATES

Figure 2 shows the time-resolved spectrum obtained from a double domain *p*-type Si(100)2×1 surface (sample 1). The energy scale is with respect to the CBM whose position is determined from the probe-only spectrum.[6] The spectrum at

TABLE I. Sample specifications.

Sample #	Crystal face	Miscut (degree)	Dopant	Doping density (cm^{-3})	Resistivity (Ω cm)
Sample 1	100	$<\pm0.5$	B(*p*-type)	10^{15}	15~30
Sample 2	100	9	P(*n*-type)	1.2×10^{13}	350
Sample 3	100	$<\pm0.5$	Sb(*n*-type)	$>2\times10^{18}$	0~0.02

$T=-1.8$ psec consists mainly of two-photon photoemission with the probe beam which can be considered as a constant background and can be subtracted from each spectrum to show the two-color spectrum more clearly. At $T=0.0$ psec at which the probe beam is in a temporal overlap with the pump beam, there is an appreciable yield increase especially at kinetic energies ranging from -0.8 to 0.5 eV. As has been shown by earlier studies, there is a strong emission from states inside the bulk band gap.[8] For these band-gap states, there is also a very fast decay at early time delays. This rapid decay in electron yield for states right below the conduction-band minimum has been observed in previous studies[6,8] and it was attributed to a fast relaxation inside the upper intrinsic surface states. However, the nature of the initial states observed in the time-resolved photoemission and the origin of the fast decay for states above CBM has remained unclear until now.

The nature of the initial states can be studied by probing their symmetry property. It is well known that the upper intrinsic surface state of Si(100)2×1 surface has odd symmetry while the lower surface state has even symmetry with respect to the mirror plane bisecting the Si dimer.[12] With the transition probability written as

$$P \propto |\langle \psi_i | \mathbf{p} \cdot \hat{e} | \psi_f \rangle|^2,$$

the symmetry principle requires that the matrix element remain invariant under the reflection with respect to the mirror plane. For a photoelectron to be detected in the electron detector lying on the mirror plane, the final state has to be even under the reflection with respect to the mirror plane. When the probe beam polarization lies in the mirror plane, the term $\mathbf{p} \cdot \hat{e}$ is even under the reflection. Therefore, the whole matrix element is odd under reflection with respect to the mirror plane. It means that the transition probability for this process is identically zero. In other words, when the dimers are aligned in such a way as to produce a mirror plane parallel to the optical table and the probe beam polarization lies in the mirror plane, the photoemission probability from the upper surface states with odd symmetry is zero.

On a single domain Si(100)2×1 surface, the Si dimers are known to form in a preferential direction, allowing study of symmetry properties with respect to the dimer axis. A single domain Si(100)2×1 surface has been prepared from a low doped *n*-type sample with 9 degree miscut (sample 2). After the cleaning, the 2×1 LEED pattern with missing half integral spot in the horizontal direction confirms that the sample is composed of a single domain with the Si dimer axis perpendicular to the optical table. When the time-resolved photoemission spectra were taken from the single domain Si(100)2×1 surface with probe beam polarization parallel to the optical table, there was no readily noticeable difference in the shape of the spectrum and its dynamics compared to those observed in the double domain surface. This indicates that the observed initial states lack the mirror symmetry which is associated with 2×1 reconstruction. Hence, it is more probable that the states observed in time-resolved photoemission are related to the defect states on the Si(100)2×1 surface as concluded in ultraviolet photoemission spectroscopy and inverse photoemission spectroscopy study on a Si(100)2×1 surface performed by Martensson and co-workers.[13,14] The presence of surface defects such as missing dimer defects on the Si(100)2×1 surface and their electronic properties have been studied by researchers employing scanning tunneling microscopy.[15] For example, authors of Ref. 15 reported that the average surface defect density on Si(100)2×1 surface is approximately 5% with sample-to-sample variation to some extent. They classified defects in Si(100)2×1 into so-called type-A, type-B, and type-C defects. Among them, the most common defects are type-C defects that break the mirror symmetry with respect to the plane bisecting the Si surface dimers. However, more careful study is needed to relate the defects observed in the scanning tunneling microscopy study to the peak in the photoemission spectra.

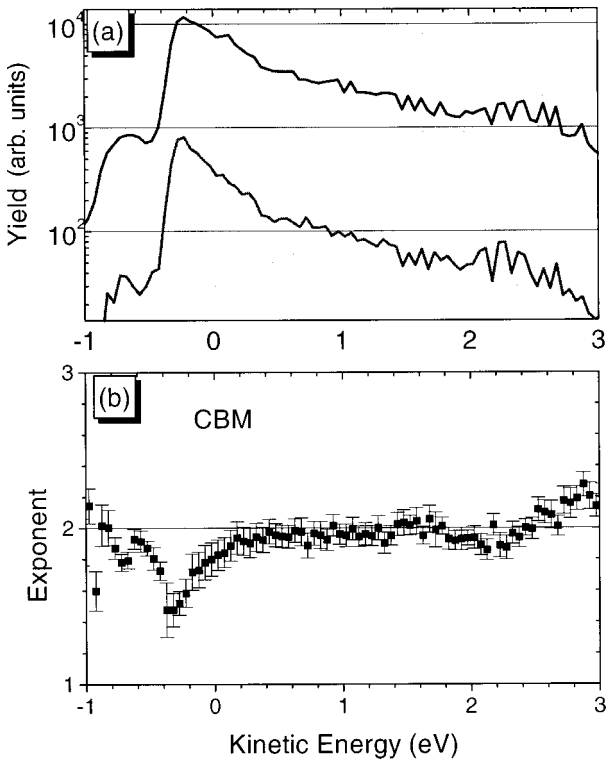

FIG. 3. (a) Spectra with 266 nm only from heavily doped *n*-type sample with two different laser intensities; (b) optimum exponent at each energy position.

The assignment of the peak below the CBM to a defect related structure on the Si(100)2×1 surface can be given further support by showing that this state can be observed via one-photon photoemission from a heavily doped *n*-type sample as was done in Ref. 13. In a heavily doped *n*-type sample, the bulk Fermi level moves close to the conduction-band minimum. The surface states close to the conduction-band minimum are occupied with electrons, if there is no strong surface Fermi-level pinning, which is the case for the Si(100) surface as confirmed by the absence of the photovoltage shift.[8] When the state is occupied by electrons, it can be observed with one-photon photoemission with a 4.66 eV probe beam.

To verify whether this is the case, fourteen photoemission spectra were taken from a heavily doped *n*-type sample (sample 3) with different intensities of the 4.66 eV beam. Figure 3(a) shows two of the fourteen spectra with third-harmonic intensities differing by a factor of 6.1. At each energy position, the electron yield can be plotted with the

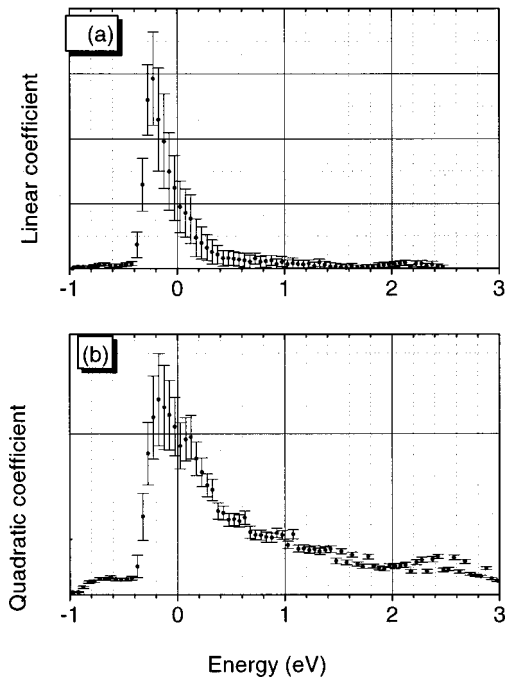

FIG. 4. (a) One-photon photoemission coefficient; (b) two-photon photoemission coefficient.

probe beam intensity and the relation of yield versus probe beam intensity can be fitted with a power law considering the exponent as the fitting parameter. The optimum exponent at each energy position is shown in Fig. 3(b). Clearly, the electrons at high energy are generated from the two-photon absorption of the probe beam as is well known from previous studies.[6,8] The exponent around the conduction band minimum is less than 2, which shows that the electron yield around the peak is a mixture of one-photon photoemission and two-photon photoemission.

To determine the relative magnitude of the one-photon photoemission process and the two-photon photoemission process, the electron yield at each energy position is fit with the following relation:

$$Y = AI + BI^2,$$

where I is the third-harmonic intensity, A is the one-photon photoemission coefficient, and B is the two-photon photoemission coefficient. The best-fit values of coefficients A and B at each energy position are displayed in Figs. 4(a) and 4(b). The yield around the peak cannot be well fitted with the above expression, which is manifested by the relatively large size of the error bars. The reason is because at that energy position one-photon photoemission and two-photon photoemission occur at the same time, giving rise to complications due to the simultaneous population change.

From the pump-and-probe photoemission spectra from a heavily doped n-type Si(100)2×1 sample, one can compare the relative contribution to the photoemitted electrons from carriers from the doping and photogenerated carriers. Figure 5 shows the pump-and-probe spectra taken from the heavily doped n-type sample at $T=0.0$ psec and $T=-4.0$ psec. The spectrum at $T=0.0$ psec has a contribution from optically generated carriers plus the electrons in equilibrium with the bulk doping of $2\times10^{18}\,\mathrm{cm}^{-3}$. However, the spectrum at $T=-4.0$ psec has the contribution only from the surface defect states *in equilibrium with* the bulk doping. The two spectra merge approximately at 0.9 eV. The two-color signal occurs only at energy positions of 0.9 eV or below. At the energy position of -0.3 eV where the peak occurs, the two-photon photoemission yield at $T=0.0$ psec is about 13 times greater than that of $T=-4.0$ psec spectrum. The photogenerated carrier density with an irradiation of an 800-nm beam with the fluence level of 1 mJ/cm^2 is approximately $3\times10^{18}\,\mathrm{cm}^{-3}$, which is comparable to the bulk doping level of the sample. The fact that the spectrum at $T=0.0$ psec shows 13 times greater peak strength than that at $T=-4.0$ psec (which includes contribution from bulk doping only) indicates a substantial departure from the equilibrium between the surface defect state and bulk states after laser light illumination. This departure implies that the optical transition matrix element for the defect state is substantially higher than for the bulk states. This kind of optical enhancement is not unreasonable at all because the arrangement at the surface is different from that of the bulk and the optical and electrical properties can be different from those of the bulk. Surface-state induced optical anisotropy on Si(100)2×1 surface is a well-known example.[16]

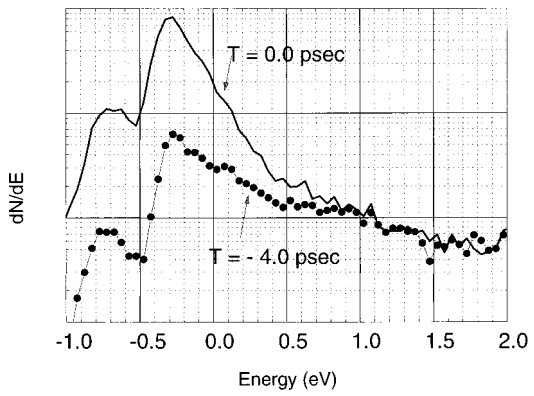

FIG. 5. Time-resolved spectra from a heavily doped n-type sample.

The nature of the optical transition involved in the photoemission process and the role of phonons in the carrier dynamics can be studied by investigating the photoemission spectra taken at different substrate temperatures.[17] Because the typical optical phonon energy is less than 50 meV,[18] the change in substrate temperature modifies the equilibrium population of the optic phonons significantly. Therefore any change in the photoemission spectra due to the optic phonons will manifest itself as the substrate temperature is changed. To study the role of phonons in the optical excitation process and the carrier dynamics, time-resolved photoemission experiments are performed on a clean silicon sample held at two different temperatures. The temperature of the sample is maintained at a constant level by flowing an appropriate amount of dc current through the electron-beam heater filament. The sample specimen plate is heated due to the radiation from the electron-beam heater filament. The voltage drop between the two ends of the filament is measured to be 5 V with the current of 1.8 A. It gives rise to a static electric field but it is shielded out by the sample specimen plate. By this method, the temperature of the sample can be varied from 300 to 600 K.

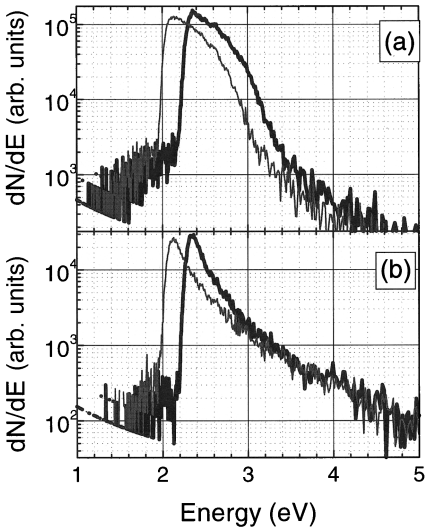

FIG. 6. (a) Spectra at two different substrate temperatures at $T=0$ psec time delay; (b) spectra at two different substrate temperatures at $T=-4.0$ psec time delay. The thick line denotes the spectrum at 600 K and the thin line at 300 K.

Time-resolved photoemission spectra are taken at 600 and 300 K from a sample of light *n*-type (sample 2). Figure 6(a) shows the spectra at $T=-4.0$ psec and Fig. 6(b) shows the two-color signal at $T=0.0$ psec for two different substrate temperatures. A uniform horizontal shift of magnitude 200 meV is observed between spectra taken at two different substrate temperatures for both time delays. The uniform energy shift is due to the Fermi-level shift of the sample at two different temperatures. The amount of the shift agrees well with the estimate of the Fermi-level shift at two different temperatures. The spectra at negative time delays and $T=0.0$ psec are similar in their magnitude and spectral shape. Figure 7 shows the magnitude of two-color signal as a function of the time delay between the pump and probe for the two temperatures. The magnitude of two-color signal is defined as the total number of electrons at each time delay minus the number of background electrons. The magnitude of two-color signal is almost the same for early time delays regardless of the substrate temperature, while it shows an appreciable difference at longer time delays. The fact that the $T=0.0$ psec spectrum is independent of the substrate temperature suggests that the phonon is not involved either in the carrier generation process or the photoemission process itself.

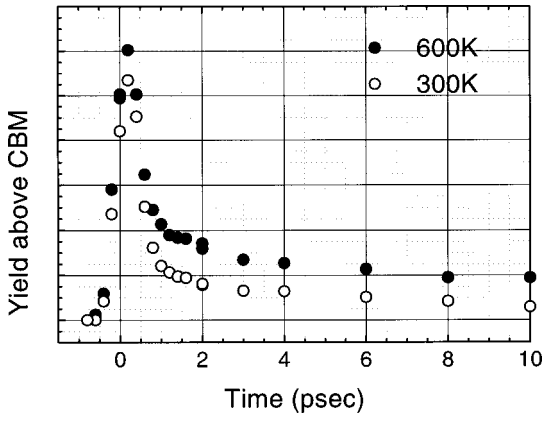

FIG. 7. Magnitude of the two-color signal as a function of pump probe delay at two different substrate temperatures.

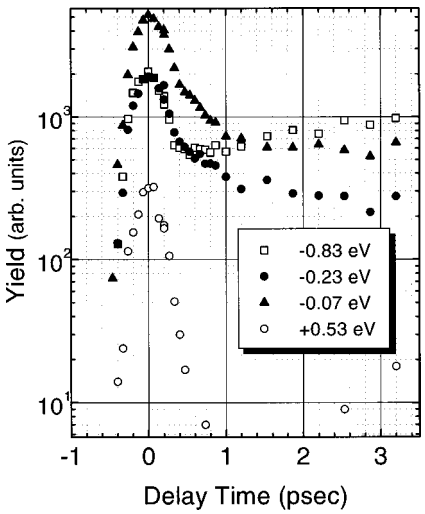

FIG. 8. The photoemission yield as a function of pump probe time delay at different energy positions.

On the other hand, the electron yield at 600 K is higher than that at 300 K at time delays longer than 0.5 psec. It can be explained by the exchange of carriers between the bulk states and the defect states that are being observed. It is well known that the optical absorption coefficient increases as the substrate temperature is increased.[19] There is little doubt that the density of carriers generated in the bulk at the substrate temperature of 600 K is approximately twice as large as that of 300 K. The coupling between the defect states and the bulk states should establish a balance of the carrier density between those two states at sufficiently long time delays. Therefore, the carrier density at the defect site is shown to be balanced at the level proportional to that of the bulk carrier density at sufficiently long time delays.

IV. ELECTRON TEMPERATURE AT VARIOUS TIME DELAYS

In previous sections, it was shown that the initial states observed in this photoemission experiment are related to defects on the Si(100)2×1 surface and that there is a substantial departure from equilibrium in carrier density near the surface. The equilibrium between the surface defect state and bulk state is established by the diffusion of carriers into the bulk states at later times. In the present section, based on these interpretations, the time-resolved spectra from a clean *p*-type Si(100)2×1 surface will be analyzed in detail and a simple model will be established for its interpretation. Some of the time-resolved spectra are shown in Fig. 2.

In Fig. 8, the electron yields at selected energy positions are displayed in a logarithmic scale as a function of the time delay to show the dynamic feature more clearly. The energy is referenced to the bulk conduction band minimum. The background spectrum has already been subtracted. At 0.5 eV above the conduction band minimum, the yield follows the laser temporal profile because the relaxation time is short for those states due to a large phase space for relaxation.[20] For states around and below the conduction-band minimum,

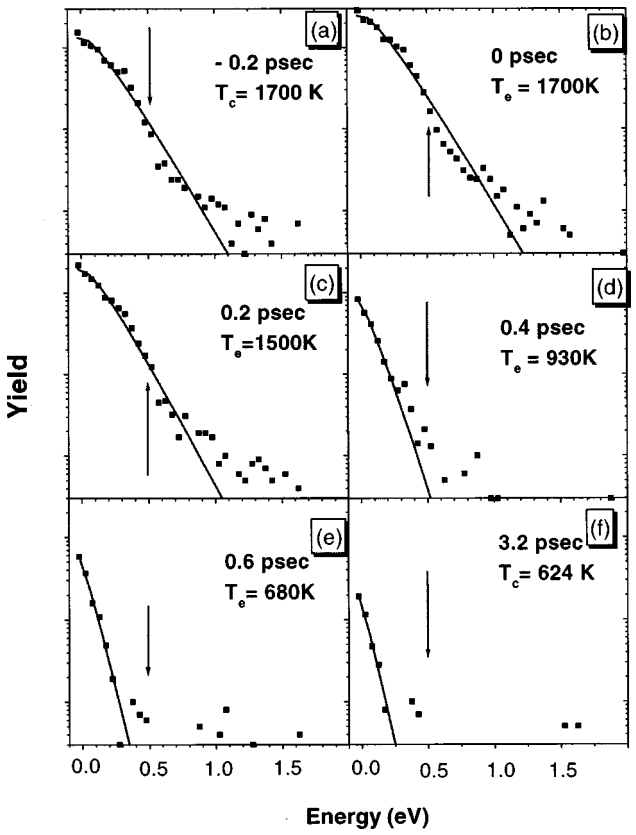

FIG. 9. Electronic distribution function above the conduction-band minimum. The solid line represents the best-fit Maxwell-Boltzmann distribution curve.

there is also a rapid rise following the laser profile. There is a rapid decrease in yield after $T=0.0$ psec, and this rapid decrease is followed by a slow decrease in yield at longer time delays. At 0.8 eV below the conduction-band minimum, the yield starts increasing after $T=1$ psec, due to the accumulation of electrons into these states.

As was previously mentioned, the optically generated carrier density at the defect site is far from the equilibrium with the optically generated carriers in the bulk. The excess carriers at the defect site transport to neighboring sites or into the bulk of silicon. The transport of carriers appears as the fast decay of the two-color signal after $T=0.0$ psec and it continues until the carrier density at the defect site becomes comparable to the bulk carrier density, resulting in the plateau of the carrier density at time delays longer than 0.7 psec.

Along with a fast carrier transport out of the defect states into neighboring sites, the shape of the electron energy distribution also changes on a very short time scale. Figure 9 displays the carrier distribution above the conduction-band minimum for six different time delays (-0.2, 0.0, 0.2, 0.4, 0.6, and 3.2 psec). To quantify the change in the shape of the electron energy distribution, the electron energy distribution can be fitted with the expression

$$f(E)=A^* \exp\left(-\frac{E}{k_B T^*}\right)\sqrt{E},$$

with A^* and T^* as fitting parameters. E is the kinetic energy of electrons referenced to the conduction-band minimum and the density of states is assumed to be proportional to the square root of the energy.

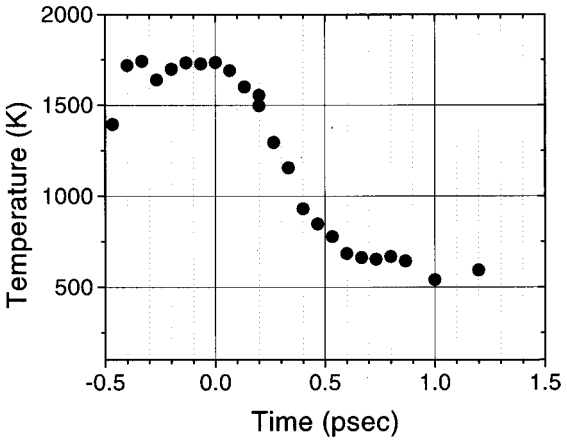

FIG. 10. Electron temperature as a function of pump probe delay time.

The best-fit electron temperatures are shown in each of the graphs. The corresponding Maxwell-Boltzmann distributions are shown with solid lines while the experimental data are shown as discrete points. At $T=-0.2$ psec and $T=0.0$ psec delay, the experimental data do not exactly fall on the solid lines: there are excess electrons below 0.5 eV and fewer electrons above 0.5 eV. This is because 0.5 eV is the one-photon absorption cutoff. In other words, 0.5 eV is the maximum kinetic energy an electron can acquire when an electron-hole pair is generated by absorption of a single 800-nm photon. Figures 9(a) and 9(b) show that the electron energy distribution is not a thermal one at $T=0.0$ psec or earlier. At positive time delays, the carrier-carrier scattering starts distributing the kinetic energy among carriers and the nonthermal feature smoothes out. After $T=0.4$ psec, the dots fall on the best-fit Maxwell-Boltzmann energy distribution except a few noisy points at high kinetic energies.

The fact that carrier-carrier scattering smoothes out a nonthermal distribution by distributing kinetic energy among carriers can also be seen in a Monte Carlo simulation of carrier dynamics in Si.[21] However, authors of Ref. 7 observed only thermal distributions inside the silicon sample, even though their time resolution was better than that of the current experiment. One possible reason is that their pump photon energy was 2.0 eV. A 2.0-eV photon generates electron-hole pairs with excess kinetic energy as large as 0.9 eV. The relaxation time for high kinetic energy carriers is extremely short, making it impossible to observe the one-photon absorption cutoff.

Aside from smoothing of the electron energy distribution, the electron temperature also changes as the time delay is increased. The electron temperatures extracted from the fit to the experimental data are displayed as a function of the time delay in Fig. 10. The peak temperature reaches 1700 K at $T=0.0$ psec, which is in good agreement with the simple estimate based on the average kinetic energy of the photogenerated carriers. The electron temperatures at negative time delays are comparable to that of $T=0.0$ psec. At negative time delays, the photogeneration is the dominant process, and the average kinetic energy of an electron is close to the value of $\hbar\omega - E_g$. Therefore the electron temperature re-

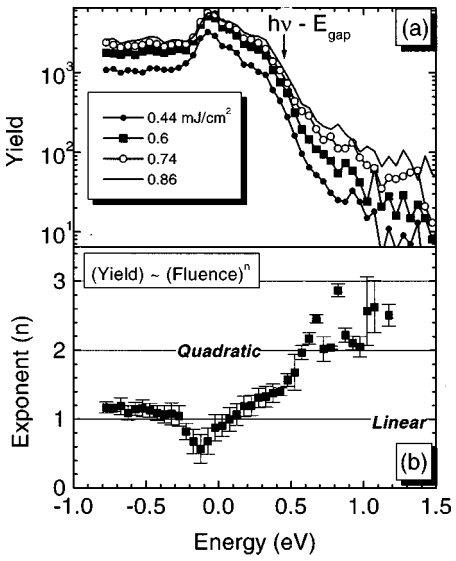

FIG. 11. (a) Electron distribution at $T=0.0$ psec with four different pump fluences; (b) optimum exponent at each energy position.

mains close to 1700 K at $T<0.0$ psec. The electron temperature becomes stabilized at 600 K at time delays later than 0.7 psec. The reason why the steady-state temperature is apparently higher than 300 K is because of limited ($\sim$50 meV) energy resolution of the electron spectrometer.

The electron energy distribution and the electron temperature can depend on the pump beam fluence incident on the sample. The relationship between pump beam fluence and the electron temperature can reveal the mechanism how the energy of the optical beam is transferred to the electrons. The current section discusses the time-resolved photoemission spectra taken at four different pump fluences: 0.44, 0.6, 0.74, and 0.86 mJ/cm^2. The pump beam fluence is varied by a combination of a half wave plate and a polarizer as described in the Sec. II. Figure 11(a) shows the spectra at $T=0.0$ psec for four different pump beam fluences on a logarithmic vertical scale. For each spectrum, the corresponding background spectrum has already been subtracted. The horizontal energy scale is with respect to the conduction-band minimum. At all pump beam fluences, the electron spectrum reaches far beyond the one-photon absorption cutoff which is 0.5 eV above the conduction-band minimum.

At each energy position, the yield versus the pump beam fluence can be fit with a power-law dependence. The optimum exponent at each energy position is shown in Fig. 11(b). The error becomes larger at higher energy due to fewer electron counts. The yield depends linearly on the pump beam fluence at lower energies, which is indicated by an exponent close to 1.0. The yield varies quadratically with the pump beam fluence above 0.5 eV, which agrees well with the one-photon absorption cutoff. Therefore the electrons with kinetic energy greater than 0.5 eV are generated with two-photon absorption of the pump beam. The two-photon absorption feature and the hot-electron tail are clearly visible even at the lowest fluence 0.44 mJ/cm^2. The electrons with kinetic energy between 0.0 and 0.5 eV are generated partly via one-photon absorption and partly via two-photon absorption, which is indicated by an exponent between 1.0 and 2.0.

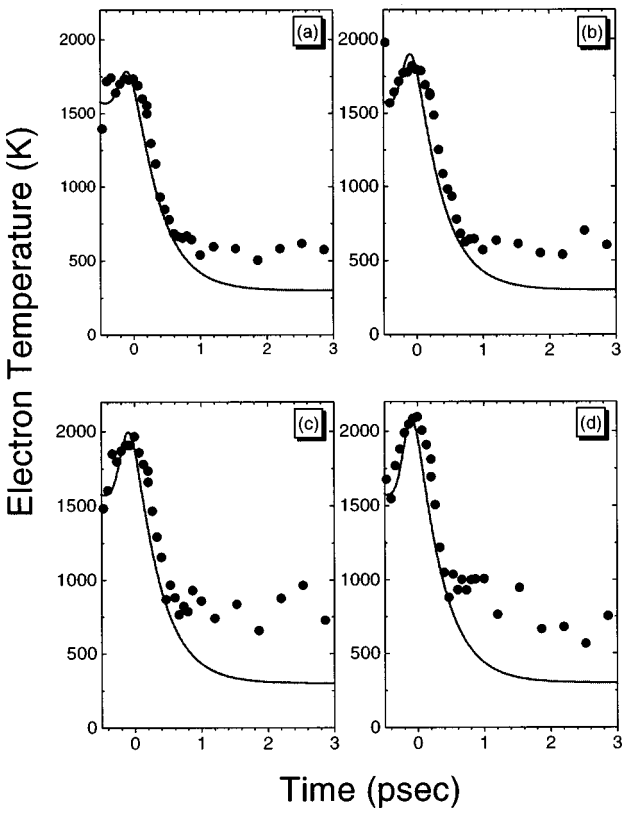

FIG. 12. Calculated electron temperatures vs experimentally determined electron temperatures at different pump beam fluences.

Another interesting feature is a saturation below the conduction-band minimum, which is indicated by the exponent less than one. The saturation occurs exactly where the electron energy distribution peaks. As a matter of fact, around the energy position of the peak, the data cannot be properly fit by a power-law dependence. The saturation of the optical pumping at the peak of the distribution agrees well with the notion that there is a strong optical enhancement into these states.

When two pump photons are absorbed for creating an electron-hole pair, the excess kinetic energy imparted to the pair becomes as high as 2.0 eV per pair, compared to 0.5 eV for one-photon absorption process. Therefore, the electron distribution can reach appreciably higher temperature when two-photon absorption is included. The electron temperature also depends on the pump beam fluence if two-photon absorption is a dominant process. Figure 12 shows the electron temperatures extracted from the experimental data at different pump beam fluences as a function of the time delay. The peak temperature occurs at $T=0.0$ psec for all fluences and it depends on the pump fluence. It reaches 2100 K with the highest pump fluence (0.86 mJ/cm^2) while it is 1700 K for the lowest fluence (0.44 mJ/cm^2). However, the temperature at $T=-0.5$ psec does not depend on the pump beam fluence because the pump beam intensity at that time delay is so low that linear absorption is dominant. At all fluence levels, the electron temperature reaches a plateau in less than 0.5 psec.

Even though the density of photogenerated carriers undergoes a rapid change near the surface after $T=0.0$ psec, the temporal change of the electronic temperature can be attributed to the energy transfer from the carriers to the lattice.

The decay of the electron temperature within 0.5 psec suggests that the carrier energy relaxation occurs on a time scale comparable to the pulse width of the incident laser. A simple and illustrative theoretical model is now proposed to extract transport parameters such as electron energy relaxation time. The model should incorporate the electron temperature dependence on the pump fluence and the fast transport of carriers out of the defect state. The model is based on the two-temperature model which has previously been applied to explain the optical properties of silicon irradiated with picosecond laser pulses.[22] It consists of a set of balance equations: the continuity equation for the carrier transport, the laser beam attenuation, and energy balance equation for the carriers and the lattice. The equations used in Ref. 22 are displayed below for discussion.

$$\frac{\partial N}{\partial t}+\nabla\cdot\mathbf{J}=G+R, \quad \text{continuity equation,}$$

$$\frac{dI}{dx}=-\alpha I-\beta I^2-\Theta NI, \quad \text{laser beam attenuation,}$$

$$\frac{\partial}{\partial t}U+\nabla\cdot\mathbf{W}=S_U-L_U, \quad \text{carrier energy balance,}$$

$$\frac{\partial T}{\partial t}=C_L\nabla\cdot\kappa_L(\nabla T)-L_U, \quad \text{lattice heat diffusion.}$$

In these equations, N is the carrier density, $\mathbf{J}$ is the current density, G is the generation rate, R is the recombination rate, I is the intensity of the laser, α is the linear absorption coefficient, β is the two-photon absorption coefficient, Θ is the free-carrier absorption cross section, U is the carrier energy density, $\mathbf{W}$ is the ambipolar energy current, S_U is the source of the total carrier energy from the laser beam, and L_U is the loss rate of carrier energy to the lattice.

In Ref. 22, it was assumed the carriers reach a quasiequilibrium among themselves which is characterized by a single carrier temperature. This assumption is not strictly true for the time scale that is being discussed in this paper because a nonthermal electron energy distribution is observed at time delays close to $T=0.0$ psec. However, to provide a starting point for the theoretical modeling of the ultrafast carrier dynamics in silicon, it is assumed that the carrier distribution can be described by a single quasithermal electron temperature T_C. Based on this assumption, the carrier energy density and the loss rate of the carrier energy to the lattice can be expressed as

$$U_C=N(E_g+3k_BT_C),$$

and

$$L_U=\frac{3Nk_B}{\tau_c}(T_C-T_L),$$

respectively. τ_c is the carrier energy relaxation time. Furthermore, it is assumed that the lattice temperature change can be neglected on the time scale of interest and it can be taken to be 300 K.[10] Because the absorption depth of the 800-nm pump beam is much greater than the probing depth of the 266-nm beam, the spatial dependence of the laser intensity due to photogeneration of carriers, the diffusion of carriers, and the lattice heat diffusion are neglected.

Due to an optical enhancement and carrier transport to the neighboring defect sites or into the bulk states, the observed electron density decreases very fast. The fast decay is simulated by putting a term $-N/\tau_0$ in the continuity equation for the carrier density. The electron transports occurs with the transport of energy. To account for the energy loss accompanying the carrier transport, a term $-(N/\tau_0)(E_g+3k_B/T_C)$ is added to the energy balance equation. τ_0 is the time for the carrier transport and it can be determined from the plot of the density of the electrons above the conduction-band minimum versus the time delay.

Based on these assumptions, the four partial differential equations used in Ref. 22 are reduced to two ordinary differential equations:

$$\frac{dN}{dt}=\frac{\alpha I+0.5\beta I^2}{\hbar\omega}-\frac{N}{\tau_0},$$

$$\frac{dU_C}{dt}=-\frac{3Nk_B}{\tau_C}(T_C-T_L)+\alpha I+\beta I^2-\frac{N}{\tau_0}(E_g+3k_BT_C).$$

These two ordinary differential equations are numerically solved to calculate the carrier density and the carrier temperature as a function of the time delay for different laser fluences. With an appropriate choice of the fitting parameters, a reasonable fit with four different curves is achieved. The calculated electron temperature is displayed for four different fluences in Fig. 12 with the experimental data displayed for comparison. The fitting parameters for the solid lines in Figs. 12(a)–12(d) are $\tau_C=0.4$ psec, $\tau_0=0.2$ psec, and $\beta=120$ cm/GW. The value for β is approximately 3–5 times greater than the value expected based on the experimental data available at other wavelengths.[23] The difference might come from the uncertainty in the measurement of the laser fluence and the simplicity of the model itself. Considering the simplicity of the model, the value for τ_C is in reasonable agreement with the value of 0.27 psec obtained through a dc transport measurement on a short channel device[24] or with the value of 0.32 psec obtained with a Monte Carlo simulator.[24]

V. CONCLUSION

We showed that the population of electrons and the shape of the electron energy distribution near the surface changes on a very short time scale after laser illumination. A pronounced peak has been observed near the bottom of the conduction band. Our study of the polarization properties of this peak revealed that it is associated with surface defect states. We also showed that there is an enhanced optical transition into the defect state compared to the bulk optical transition and that the defect state exchanges carriers with bulk states on a very short time scale.

We studied the carrier distribution at various pump beam fluences, and found that the pump beam photons are absorbed by carriers through both one-photon absorption and two-photon absorption. The two-photon absorption is responsible for high kinetic energy electrons inside the conduction band. The energy relaxation time for these electrons

is much shorter than the temporal resolution of the current experiment. The initial energy distribution of photogenerated carriers is observed to be nonthermal with a drop at 0.5 eV above the conduction-band minimum. It arises from the one-photon absorption cutoff. The carrier-carrier interaction smoothes out the one-photon absorption cutoff, bringing the nonthermal distribution to a thermal one. This thermalization also occurs on a very short time scale comparable to the temporal resolution of the experiment.

The more gradual change in the shape of the electron energy distribution can be characterized by the change in its electron temperature, which can be determined by fitting the experimental data with a Maxwell-Boltzmann distribution. The peak electron temperature occurs at zero time delay and it is shown to be greater than 1700 K, depending on the pump fluence. The photogenerated carriers are shown to lose their kinetic energy to the lattice at subsequent time delays. The ''relaxation'' of the kinetic energy to the steady-state value occurs on a time scale of 0.5 psec.

A simplified set of ordinary differential equations is developed to extract the energy relaxation time from the experimental data. The model includes the two-photon absorption and carrier transport into neighboring sites or into the bulk states. The calculated electron temperatures for four different pump fluences are compared with experimental data and the best-fit parameters have reasonable values. The carrier energy relaxation time has been extracted from the fit and it is determined to be 0.4 psec.

ACKNOWLEDGMENTS

This work was performed by support from the Air Force Office of Scientific Research, Air Force Material Command, USAF, under Grant Nos. F49620-97-1-0020 (Joint Services Electronics Program), F49620-93-0353 (AASERT), and F49620-94-1-0464, and the Director, Office of Energy Research, U.S. Department of Energy, under Contract No. DE-AC03-76SF00098.

[1] For discussion of hot-electron effects in electronics devices, see M. V. Fischetti, S. E. Laux, and D. J. DiMaria, Appl. Surf. Sci. **39**, 578 (1989).

[2] For discussion of the application of ultrafast lasers for study of semiconductors, see *Semiconductor Probed by Ultrafast Laser Spectroscopy*, edited by R. R. Alfano (Academic Press, Orlando, 1984).

[3] J. Bokor, R. Haight, R. H. Storz, and J. Stark, Phys. Rev. B **32**, 3669 (1985).

[4] *Modern Techniques of Surface Science*, D. P. Woodruff and T. A. Delchhar, 2nd ed. (Canbridge University Press, New York, 1994).

[5] R. Haight and J. A. Silberman, IEEE J. Quantum Electron. **QE-25**, 2556 (1989).

[6] S. Jeong, H Zacharias, and J. Bokor, Phys. Rev. B **54**, R17 300 (1996).

[7] J. R. Goldman and J. A. Prybyla, Phys. Rev. Lett. **72**, 1364 (1994).

[8] M. W. Rowe, H. Liu, G. P. Williams, Jr., and R. T. Williams, Phys. Rev. B **47**, 2048 (1993).

[9] T. L. F. Leung and H. M. van Driel, Appl. Phys. Lett. **45**, 683 (1984).

[10] S. Jeong, Ph.D. dissertation, University of California at Berkeley, 1997.

[11] S. M. Sze, *Physics of Semiconductor Devices*, 2nd ed. (John Wiley & Sons, New York, 1981).

[12] R. J. Hamers, Ph. Avouris, and F. Bozso, Phys. Rev. Lett. **59**, 2071 (1987).

[13] L. S. O. Johansson, R. I. G. Uhrberg, P. Martensson, and G. V. Hanson, Phys. Rev. B **42**, 1305 (1990); P. Martensson, A. Cricenti, and G. Hansson, *ibid.* **33**, 8855 (1986).

[14] Assuming that the electron affinity of Si(100) surface is 4.0 eV (see Ref. 8), the maximum transverse momentum that can be probed with a 4.66 eV photon is estimated to be less than 0.36 Å^{-1} for states below the conduction-band minimum. It is not large enough to reach the J' point of the surface Brillouin zone of the Si(100)2×1 surface where the band dispersion is greatest (see M. Rohlfing, P. Kruger, and J. Pollmann, Phys. Rev. B **52**, 1905 (1995), and references therein). Therefore the experimentally observed peak is located near the Γ point of the surface Brillouin zone.

[15] For example, see R. J. Hamers and U. K. Köhler, J. Vac. Sci. Technol. A **7**, 2854 (1989), and references therein.

[16] T. Yasuda, L. Mantese, U. Rossow, and D. E. Aspnes, Phys. Rev. Lett. **74**, 3431 (1995).

[17] R. Haight and M. Baeumler, Phys. Rev. B **46**, 1543 (1992).

[18] J. Singh, *Physics of Semiconductors and Their Heterostructures* (McGraw-Hill, New York, 1993).

[19] E. H. Sin, C. K. Ong, and H. S. Tan, Phys. Status Solidi A **85**, 199 (1984).

[20] P. D. Yoder and K. Hess, Semicond. Sci. Technol. **9**, 852 (1994).

[21] C. Jacoboni, *Proceedings of the 13th International Conference on Physics of Semiconductors*, edited by F. G. Fumi (Marves, Roma, 1976).

[22] H. M. van Driel, Phys. Rev. B **35**, 8166 (1987).

[23] D. H. Reitze, T. R. Zhang, W. M. Wood, and M. C. Downer, J. Opt. Soc. Am. B **7**, 84 (1990).

[24] D. Sinitsky, F. Assaderaghi, H. Orshansky, J. Bokor, and C. Hu, Solid-State Electron. **41**, 1119 (1997).